Ceramics International 23 (1997) 425–436

PII: S0272-8842(96)00051-X
0272-8842/97/$17.00 + .00

Oxidation of Polycrystalline α-Silicon Carbide Ceramic

Dean-Mo Liu

Materials Research Laboratories, Industrial Technology Research Institute, Chutung, Hsinchu, Taiwan 31015, ROC

(Received 4 December 1995; accepted 25 March 1996)

Abstract: Oxidation behaviours and associated flexural strength of pressureless-sintered α-SiC ceramic, with Al_2O_3 and Y_2O_3 as sintering additives, were investigated in the temperature range of 1200–1350 °C at 50 °C intervals. The oxidation kinetics typically exhibited a parabolic behaviour which indicated a diffusion controlled mechanism with an activation energy ranging from 128 kJ/mol to 92 kJ/mol, decreasing monotonically with increasing additive content from 5 wt% to 20 wt%. The oxide scale was characterized in terms of microstructure and phase formation. The scale is essentially a composite structure consisting of pores, crystalline yttrium silicate and YAG phases, and amorphous silica. The flexural strength of the SiC decreases somewhat with oxidation due primarily to surface pit formation. The microstructure, particularly the initial surface morphology, of the SiC with higher additive content may also be considered as an important factor for strength behaviour after oxidation at elevated temperatures.

1 INTRODUCTION

Silicon carbide (SiC) ceramic has been recognized as a prime candidate material for high-temperature structural applications such as heat engine components, heat exchangers, etc., due to its good strength, excellent resistance to corrosion and oxidation, and high thermomechanical, as well as thermophysical, properties. The densification of SiC via pressureless sintering has been an important subject for years. Recently, Omori and Takei,[1] using alumina and yttria as sintering aids, obtained dense SiC ceramic with an improved mechanical strength of greater than ~650 MPa. More recently, Lee *et al.*[2] obtained a dense SiC ceramic with high fracture toughness of ~8.3 MPa·m$^{1/2}$, by allowing exaggerated growth of the SiC grains at 2200 °C to form a microstructure containing considerable amounts of plate-like α-SiC grains. In a recent communication,[3] the present author also demonstrated that SiC Al_2O_3 Y_2O_3 ceramic exhibited an excellent high-temperature flexural strength at 1200 °C in air for relatively short-term duration.

The oxidation behaviour of silicon carbide ceramics has long been an important subject for numerous materials scientists and engineers simply because of its great potential as high-temperature structural components. Typically, it is generally accepted that the oxidation behaviour of silicon carbide is controlled by diffusion of oxygen molecules through the growing oxide scale (mostly amorphous silica film) as characterized by a parabolic rate model over a wide temperature range, e.g. 1200–1500 °C. The diffusion of oxidant through the oxide scale is regarded as a rate-limiting process in many investigations in which the lower activation energy values were obtained. Numerous reports, however, depicted higher activation energy values[4–7] and concluded that the diffusion of oxidant through the amorphous silica film is not a rate-limiting process for SiC oxidation; instead, a mechanism other than oxygen diffusion dominates oxidation, e.g. the desorption of gaseous product (frequently CO) from the SiC/oxide interface. In fact, a large spectrum of activation energy values for SiC oxidation has been reported from below 100 kJ/mol to above 500 kJ/mol.[4,8,9]

Costello and Tressler[8] observed the oxidation behaviour for both sintered and hot-pressed SiC ceramics and proposed that oxidant diffusion through growing oxide scale is a rate-controlling process based on the direct observation of a platinum-marker experiment.

The activation energy values exhibit as a complex function of a number of factors, such as extent of oxide scale crystallization, amount and type of sintering additive elements, impurities, oxidation temperature, etc. Generally, crystallization of the oxide film from amorphous silica to crystalline α-cristobalite and reduction of the amount of sintering additives caused an increase in activation energy. Recently, Narushima *et al.*[10] indicated that the interstitial diffusion of oxygen ions may be responsible for high activation energy values at relatively high temperatures. However, the actual mechanism(s) of the SiC oxidation may be complex (a mixed mode is possible) and frequently became more complex when other factors such as sintering additives, scale crystalliztion, were incorporated. This usually interferes with the interpretation of the intrinsic oxidation behaviour observed experimentally. In the various investigations SiC ceramics, e.g. single crystal, chemically vapour deposited, hot-pressed, pressureless-sintered, with various additive elements have been used as a model material. Based on the promising mechanical properties of the $SiC–Al_2O_3–Y_2O_3$ ceramics in comparison with other sintered silicon carbide ceramics stated above and because of the need to understand the relevant oxidation mechanism, the oxidation behaviour, microstructural evolution of the oxide scale, along with the flexural strength after oxidation of $SiC–Al_2O_3–Y_2O_3$ ceramics were investigated.

2 EXPERIMENTAL PROCEDURES

Powder mixtures containing α-SiC (mean particle size 0.48 μm, Showa Denko, Japan) and varying amounts of Al_2O_3 and Y_2O_3 as sintering aids, with an SiC/additive weight ratio of 95/5, 90/10 and 80/20, were prepared by wet mixing (using deionized water as immersion medium) in a polyethylene jar with alumina balls as grinding medium. The Al_2O_3/Y_2O_3 ratio in each powder mixture was fixed to a value corresponding to the lowest temperature (~1850–2000 °C) required to form an eutectic melt according to the $SiO_2–Al_2O_3–Y_2O_3$ phase diagram.[11] The SiC slurry was poured into a plaster mould to form a cake. After drying at 120 °C for 16 h, the SiC cakes were sintered at 1900 °C for 2 h in Ar atmosphere; then the temperature was increased to 2000 °C for an additional 2 h.

The sintered compacts, having a density of approximately 99–99.3% (as determined by the Archimedes principle) with dimensions 3 mm×4 mm×40 mm, were sliced by a slow-speed diamond saw followed by polishing consecutively with 1 μm diamond paste. The specimen was placed on an alumina boat in an electrically heated furnace and the temperatures were kept at 1200–1350 °C in 50 °C intervals for various soaking time periods, up to 120 h, in ambient air. The weight change of the specimens due to oxidation was measured in each pre-set soaking period using an electrobalance with a sensitivity of 0.0001 g. The oxide scale was characterized using scanning electron microscopy (Cambridge Instruments, S-360), energy dispersive X-ray analysis (EDAX), and X-ray diffraction analysis (Philips).

The four-point flexural strength of the oxidized specimens was measured at ambient temperature

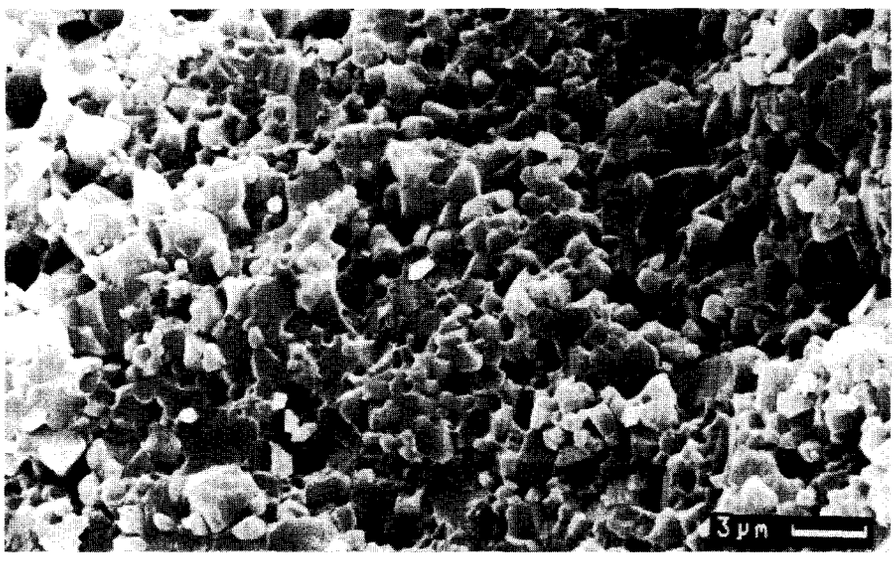

Fig. 1. Scanning electron micrograph of the fractured surface of the SiC ceramic.

Fig. 2. Transmission electron micrograph revealing the distribution of secondary phase at the multi-grain junctions.

using an Instron tester (Model 1361, with 30 mm outer span and 10 mm inner span). The cross-head speed for these tests was 0.5 mm/min. Five to seven specimens were used to determine the strength.

3 RESULTS AND DISCUSSION

3.1 Microstructure of sintered compact

The microstructural feature of the sintered SiC ceramic (with 10 wt% additive) is shown representatively in Fig. 1. The microstructure of the SiC is composed primarily of equiaxed grains with a grain size over the range of ~1–3 μm. Several small intergranular pores are clearly visualized.

Figure 2 shows a transmission electron micrograph of the microstructure of the SiC ceramic. The majority of the secondary phase in the SiC–Al_2O_3–Y_2O_3 ceramic is distributed at the three–four-grain junctions, but only a minor part is distributed along the two-grain boundaries. The secondary phase distributes as a thin layer but with different thicknesses over the SiC grains. The occurrence of the intergranular layer in the SiC–Al_2O_3–Y_2O_3 ceramic suggests that the secondary phase composition completely wets the SiC grains. The secondary phase is verified as an amorphous glassy phase over the sintering profiles as determined by electron diffraction analysis.[12]

3.2 Oxidation kinetics

The typical weight change versus soaking period curves for the oxidation of the SiC ceramics with 10 wt% additives at various temperatures are shown in Fig. 3. The parabolic oxidation curves at various temperatures for varying sintering additives are shown in Fig. 4. The experimental data for all measurements correlate well with the parabolic model over the studied temperature ranges and the entire time period for different additive fractions. The slopes of the straight lines represent

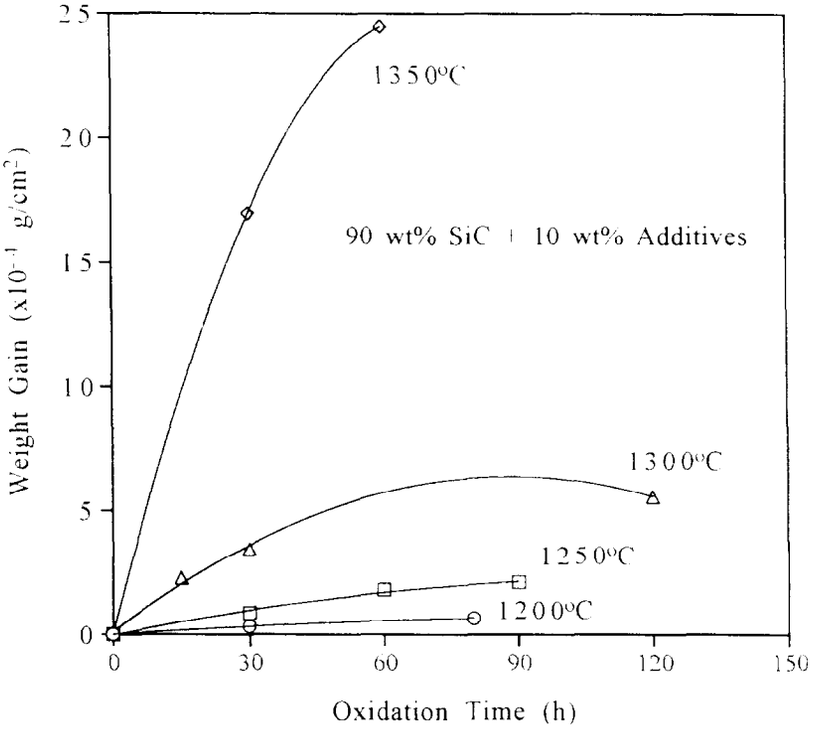

Fig. 3. Weight gain vs oxidation time in the oxidation of the SiC containing 10 wt% additives.

the apparent oxidation rate constant (K_{app}). Using the Arrhenius equation:

$$K_{app} = A \exp(-E/RT) \quad (1)$$

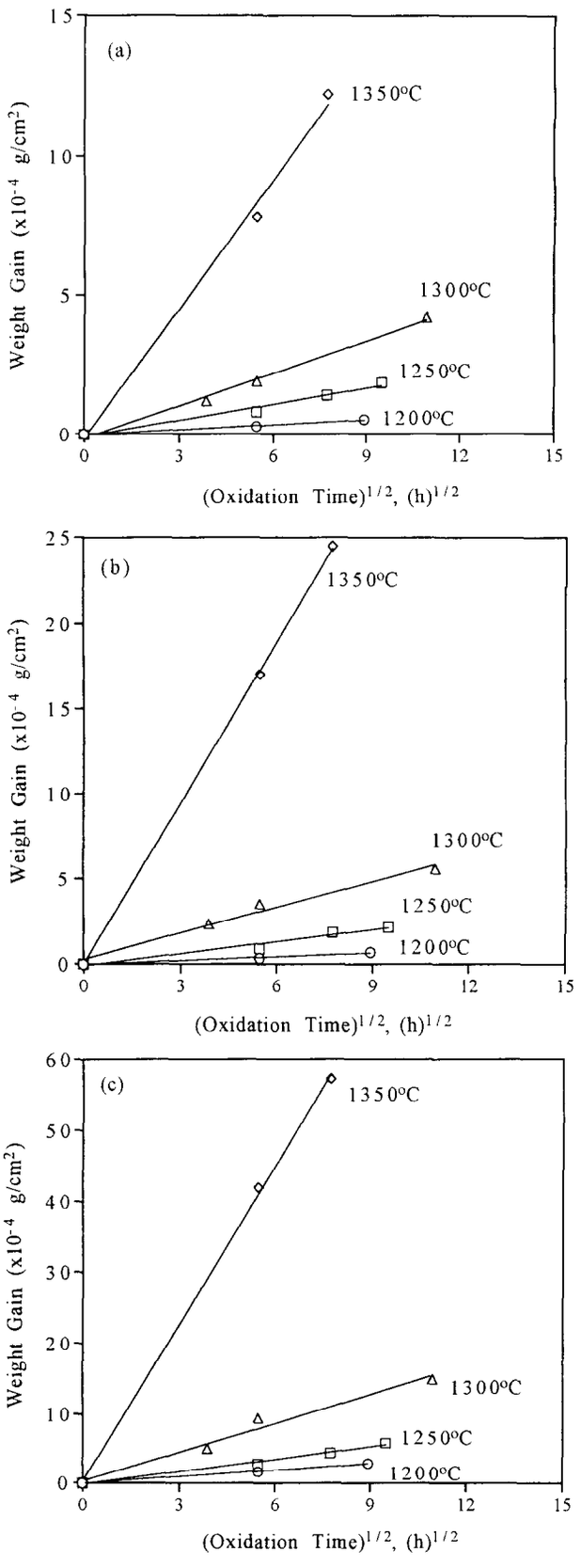

Fig. 4. Parabolic rate model for the oxidation of the SiC containing (a) 5 wt%, (b) 10 wt% and (c) 20 wt% additives.

where E is the apparent activation energy which is considered as the minimum energy for the rate-limiting step of the oxidation, R is the gas constant and T the absolute temperature. The rate constants were plotted against the reciprocal absolute temperatures, as shown in Fig. 5. Activation energies of 128 kJ/mol, 114 kJ/mol and 92 kJ/mol for additive fractions of 5%, 10% and 20%, respectively, were obtained. The activation energy values obtained for additive fractions below 20% are close to the energy value ($\sim$113 kJ/mol) required for oxygen molecules diffusion through the oxide film during the oxidation of silicon.[13] This result suggests that the oxidation mechanism for the SiC–Al_2O_3–Y_2O_3 ceramics is essentially controlled by molecular oxygen diffusion through the oxide scale in this temperature region.

The oxidation behaviour appeared to be relatively unchanged over the long-term soaking period, suggesting that the molecular oxygen diffusion mechanism is operative without significant change during prolonged soaking time. Increasing the additive fraction decreases the apparent activation energy and this agrees with numerous literature reports[4,14,15,16] that the additive and impurity elements, either intentionally added or which originally existed in the starting powders, lower the devitrification temperature of the oxide scale by reducing its viscosity. Under these circumstances, the oxygen diffusion may thus be accelerated across the oxide scale, causing an increase in the oxidation rate.

3.3 Microstructural evolution of the oxide scale

It is observed that the oxidation of SiC ceramic occurs in ambient air, wherein a silica scale is formed on the surface according to the reaction:

$$2SiC_{(s)} + 3O_{2(g)} \rightarrow 2SiO_{2(s)} + 2CO_{(g)} \quad (2)$$

The evolution of $CO_{(g)}$ and/or possible other gaseous by-products eventually causes the formation of bubbles and craters on the surface. In this study, during soaking for up to 120 h at 1200 °C, the SiC surface shows numerous pits or voids formation (Fig. 6(b)) in comparison with the unoxidized polished surface (Fig. 6(a)). X-ray diffraction analysis revealed that the oxidized surface (Fig. 6(b)) showed the presence of yttrium silicate ($Y_2Si_2O_7$) and of an amorphous phase (which is believed to be silica). No cristobalite phase has been detected. The oxidized surface was apparently roughened by pit formation. The extent of such pit formation appeared to decrease proportionally with decreasing additive content. This result can be explained

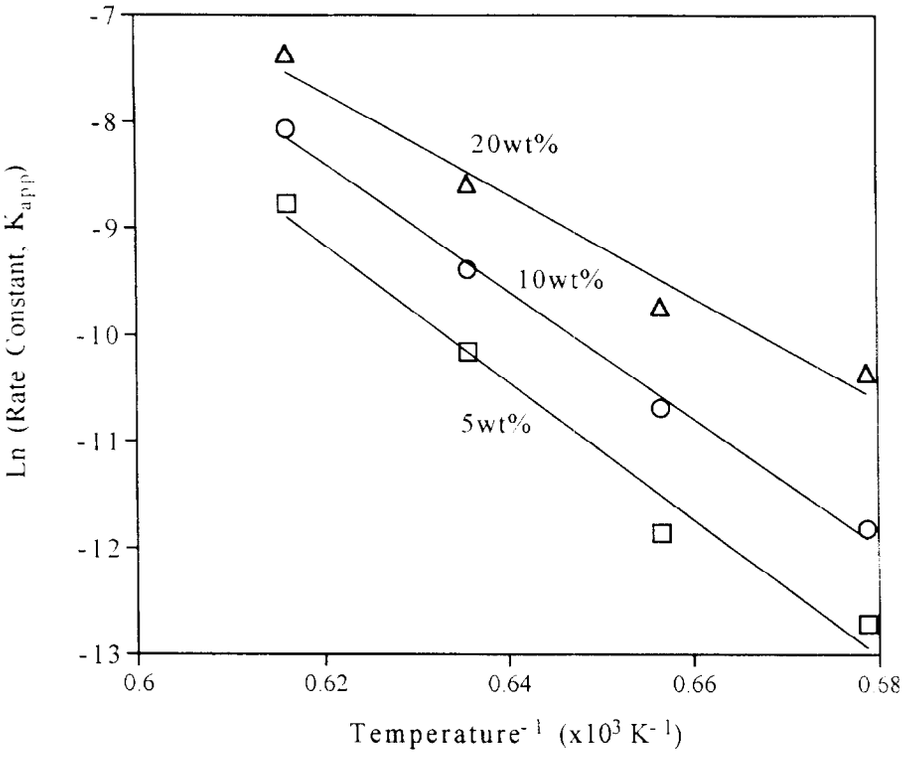

Fig. 5. Arrhenius plot of the oxidation of the SiC–Al_2O_3–Y_2O_3 ceramic with varying additive contents.

by assuming that the gaseous CO (reaction 2) was reduced primarily because of the suppression of the inward diffusion of oxygen through the highly viscous oxide scale that further limited oxidation.

At 1300 °C, the surface became rougher compared to that at 1200 °C, which is due to severe bubbling phenomena (Fig. 7). Some of the pits have a size of the order of 30 μm. This was frequently observed in the oxidation of polycrystalline SiC, as previously reported by Singhal[4] and Mieskowski *et al.*[7] Mieskowski *et al.* indicated in their investigation that the pits should result from the preferential oxidation of C inclusions; however, this may not be totally true for the present case because the C content in the starting powders was only 0.54 wt%. Instead, a vigorous evolution of the gaseous products escaping from the SiC/oxide interface to the ambient is considered to be the major cause. Part of the oxidized surface was polished with 30-μm diamond paste to remove the oxide scale and examined using scanning electron microscopy. Figure 8 illustrates a selected area showing both the oxidized surface (left side) and the SiC surface (right side) underneath the oxide scale. The pits distributed at the oxidized surface show a diameter greater by a factor of 3–5 than those of the pits underneath the oxide scale.

It may therefore be assumed that once the gaseous products form at the SiC/oxide interface, they diffuse through the scale to the ambient in a path depending possibly on gas pressure, chemical potential gradient relative to the surrounding microenvironment,[17] and the distance to the surface, followed by growing in size while moving upward to the oxide surface. This phenomenon was also observed by Schiroky in the oxidation of chemically vapour deposited SiC.[18] The presence of bubbles or pores and pits makes it rather difficult to estimate the oxide scale thickness with accuracy. The roughening effect became more significant with the increase in the oxidation temperature to 1350 °C for 30 h with 20 wt% additives, the surface was seriously damaged with the formation of large pits with dimension of 40–100 μm in diameter (Fig. 9).

A cross-sectional observation of the same specimen as in Fig. 9 shows a series of pores at the interface (Fig. 10). Some of the pores formed at the interface are interconnected (indicated by arrows), some are isolated with a size of approximately 8–10 μm in diameter. The oxide film has a thickness roughly estimated to be ~25–30 μm. However, under identical oxidation conditions, the oxide surface with only 5 wt% additives appears to be smooth and the oxide scale is essentially a composite structure containing numerous small spherical pores of ~4–6 μm in diameter distributed randomly throughout the oxide scale, as depicted in Fig. 11. The thickness of the composite oxide scale for 5 wt% additives is approximately 10 μm, which is smaller by a factor of 2–3 than that for 20 wt% additives. Since a discrete bubbles form should be

the result of rapid production and desorption of gaseous products across the scale at oxidation temperature (as illustrated in Fig. 11),[7] a sufficient amount and interconnected bubbles formed at the interface (see Fig. 10) suggested that the outward diffusion of the gaseous products is strongly suppressed. One possible reason may be due to the formation of a relatively thick oxide scale because a gas flow rate (F) per unit area of the oxide scale of thickness d can be expressed by:

$$F = K(p_2 - p_1)/d \tag{3}$$

where K is the permeation coefficient, p_1 the ambient pressure, and p_2 the gas pressure at the SiC/oxide interface. The thicker the scale, the lower the rate of the gas flow through the scale, resulting in interconnected bubbles. In this situation, the surface pits decrease in population for 20% additives in comparison with those for 5% additives (see Figs 7 and 9 for comparison). Another plausible explanation may be lower gas pressure where (p_2-p_1) value is relatively small, which, in turn, largely reduces the gas flow rate. The larger the bubble size, the lower the gas pressure according to:

$$p_2 = p_1 + 2\gamma/r \tag{4}$$

where γ is the surface energy of the oxide scale and r the bubble radius. Mieskowski *et al.* calculated the gas pressure in a 20-μm bubble as 1.3×10^5 Pa,

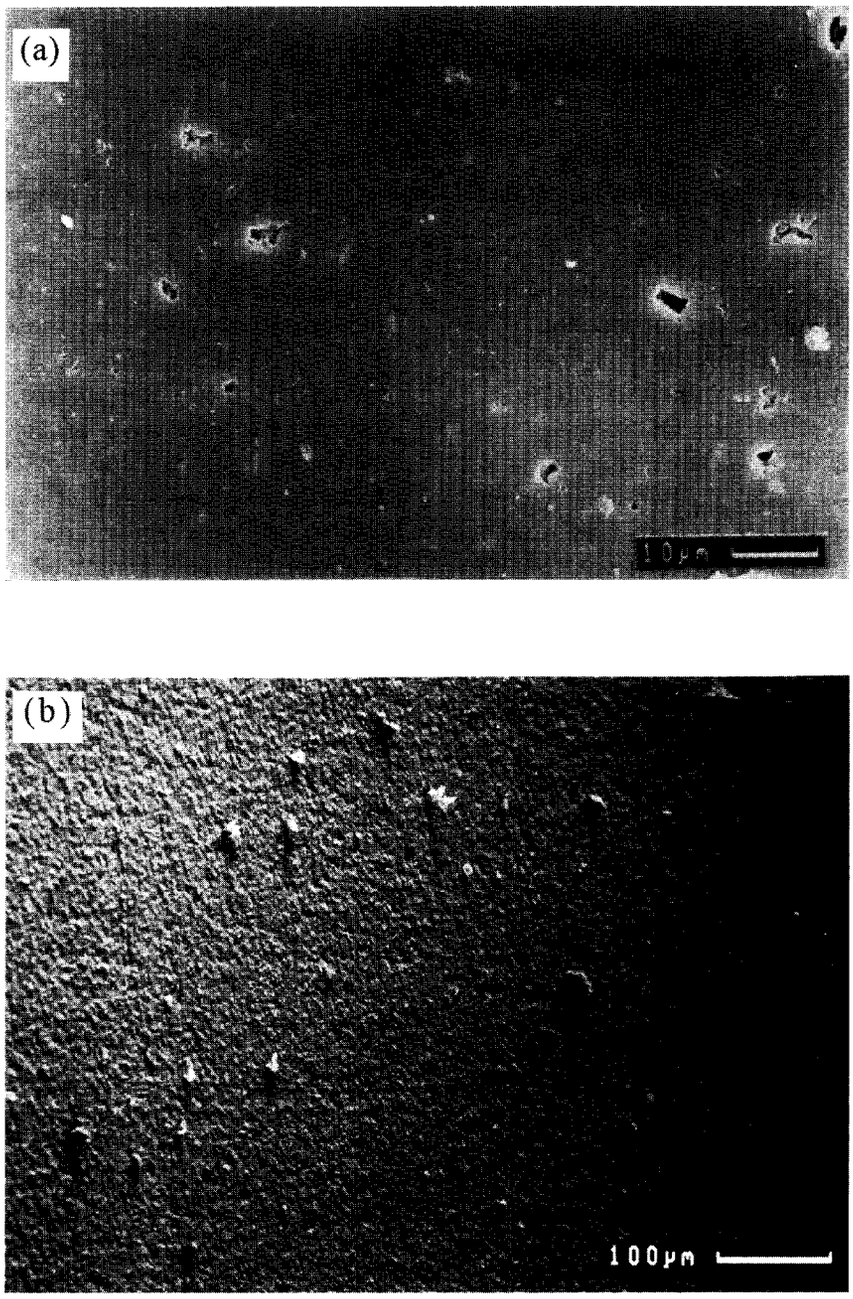

Fig. 6. Surface morphology of the SiC (a) before and (b) after oxidation at 1200 °C for 120 h.

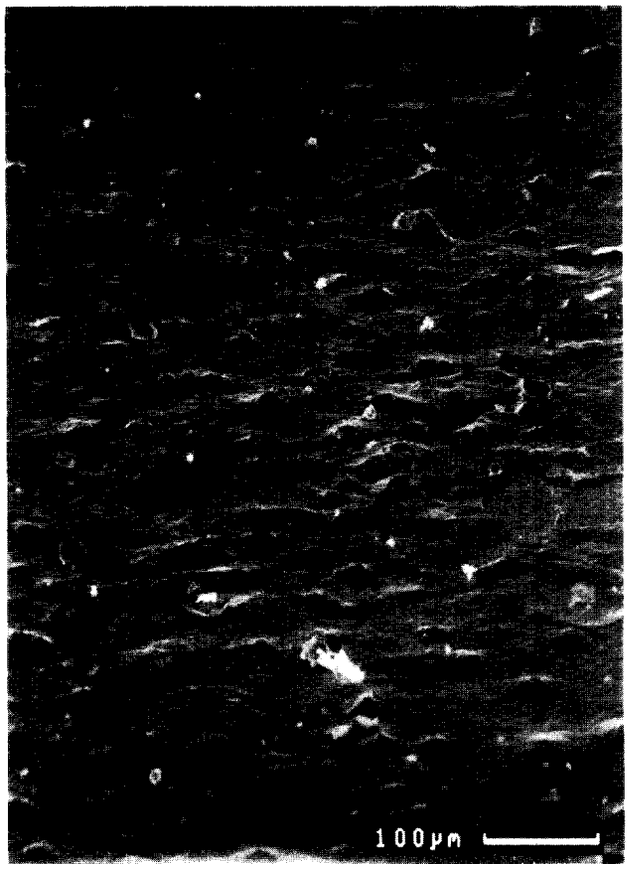

Fig. 7. Pit formation at the oxide scale after oxidation at 1300 °C.

Fig. 9. Serious surface damage with larger-sized pit formation after oxidation at 1350 °C.

which is slightly higher than the ambient pressure. The bubble size in the SiC/oxide interface is in the range of ~ 10–25 μm, corresponding to a gas pressure of 2.6×10^5–1.06×10^5 Pa by assuming $\gamma = 0.3$ J/m^2. This accordingly results in a relatively small gas flow rate. Both these factors significantly minimize the possibility of the escape of the gaseous products.

The higher content of additive elements may correspond to a lower oxide viscosity at oxidation temperature, which increases the inward diffusion of oxygen. Furthermore, the formation of a porous structure may in some way promote the diffusion of oxidant through the oxide scale for subsequent oxidation. On the basis of the above two arguments, the oxidation rate should increase and correspondingly results in a decrease in apparent activation energy as discussed in the preceding section.

One interesting phenomenological observation on the microstructure evolution of the oxide scale is the formation of needle-like material as typically

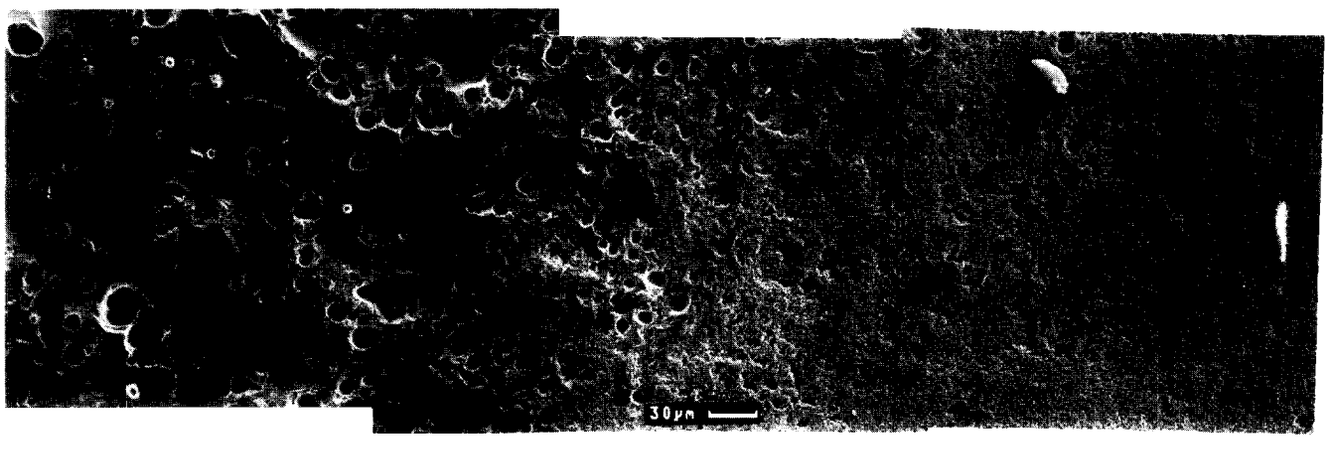

Fig. 8. Surface morphology of the oxidized SiC showing formation of the oxide scale (left side) and SiC underneath the scale (right side).

shown in Fig. 12, which is similar to that observed in the oxidation of hot-pressed Si_3N_4 by Singhal.[19] However, it has rarely been reported in SiC oxidation. It was found in this study that the presence of the needle-like crystals can be clearly visualized at temperatures $\geq 1300\,^{\circ}C$ for a prolonged soaking period. The soak time required for the formation of the needle-like crystals decreased with increasing temperature, e.g. ~ 60 h at $1300\,^{\circ}C$ and < 30 h at $1350\,^{\circ}C$. An increase in additive fractions increases the population of the needle-shaped crystals; however, no further analysis on quantitative evaluation of such a relationship has been performed. The needle-like crystals are composed primarily of yttrium and silicon elements, as determined using energy dispersive X-ray analysis (Fig. 13), and X-ray diffraction analysis confirmed the presence of an yttrium silicate ($Y_2Si_2O_7$) structure. In fact, the yttrium silicate phase has readily been formed at $1200\,^{\circ}C$ with a longer soaking period but may be in a form other than needle geometry, or may be too small to be easily visualized. It is assumed that the formation of the yttrium silicate is a result of a subsequent reaction between the amorphous SiO_2 scale and the Y_2O_3 additive, followed by the oxidation described in reaction (2) because no cristobalite phase was detectable over the entire range of oxidation conditions for all the specimens. Although, a considerable amount of Si element together with small amounts of Al and Y elements were detected, as revealed by the EDAX, Fig. 14. These needle-like crystals have dimensions of

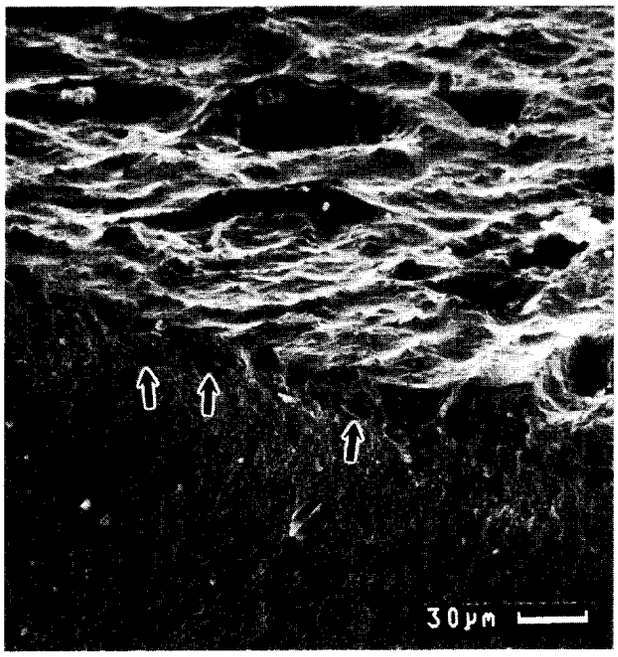

Fig. 10. Interconnected and larger pores formed at the SiC/oxide interface when the SiC with 20 wt% additives was oxidized at $1350\,^{\circ}C$ for 30 h.

Fig. 11. Spherical pores distributed randomly in the oxide scale formed by oxidation of the SiC with 5 wt% additives at $1350\,^{\circ}C$ for 30 h.

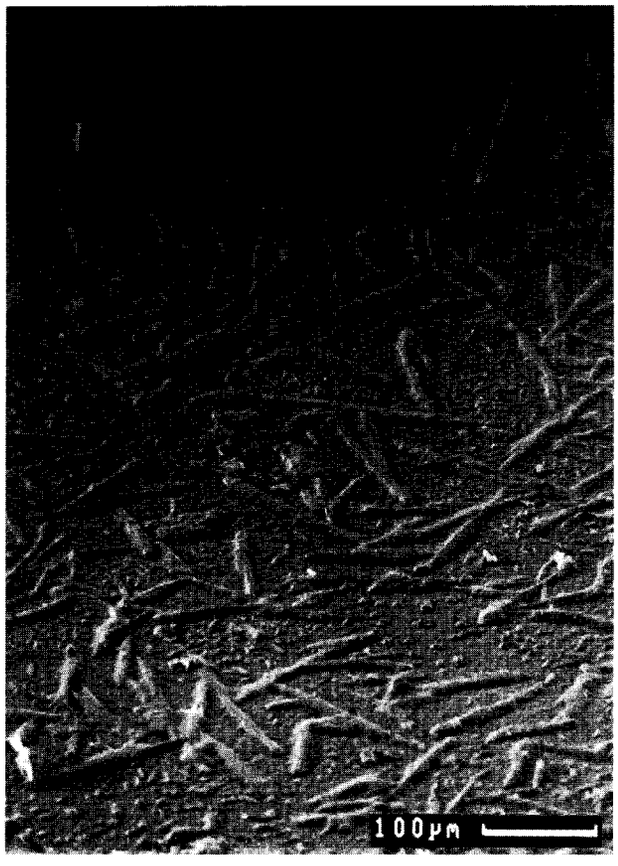

Fig. 12. The presence of the needle-shaped crystals on the oxide scale after oxidization at $1300\,^{\circ}C$ for ~ 60 h.

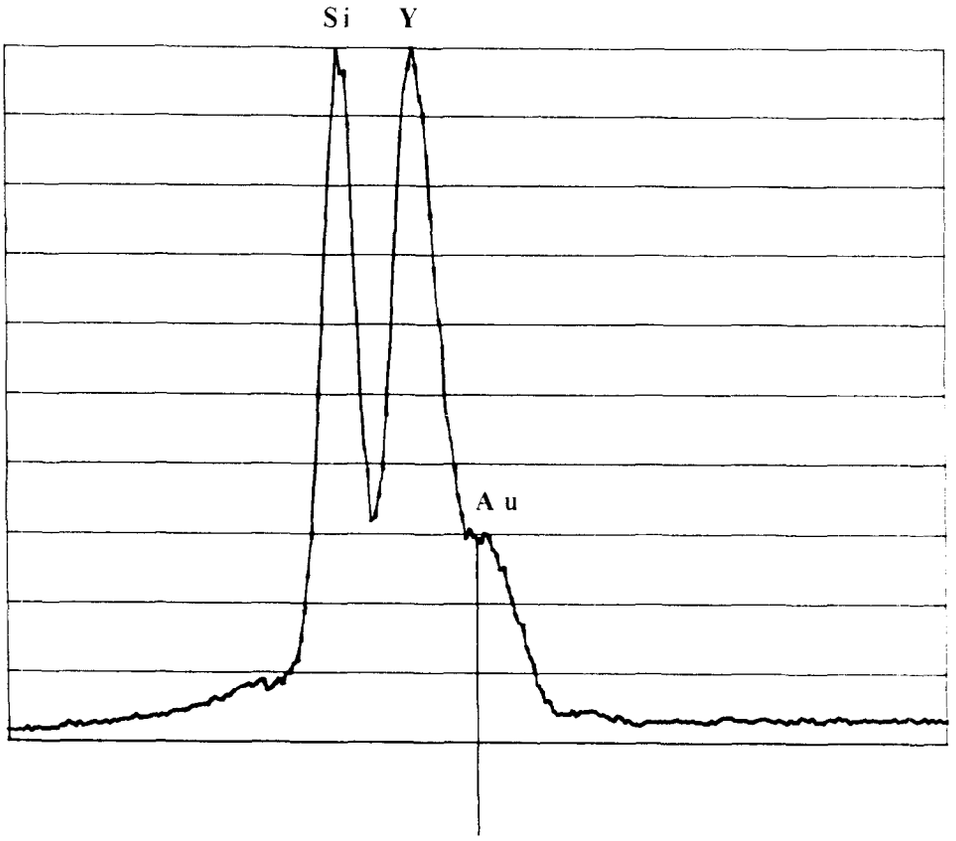

Fig. 13. EDAX analysis of the needle-shaped crystals containing Si and Y elements.

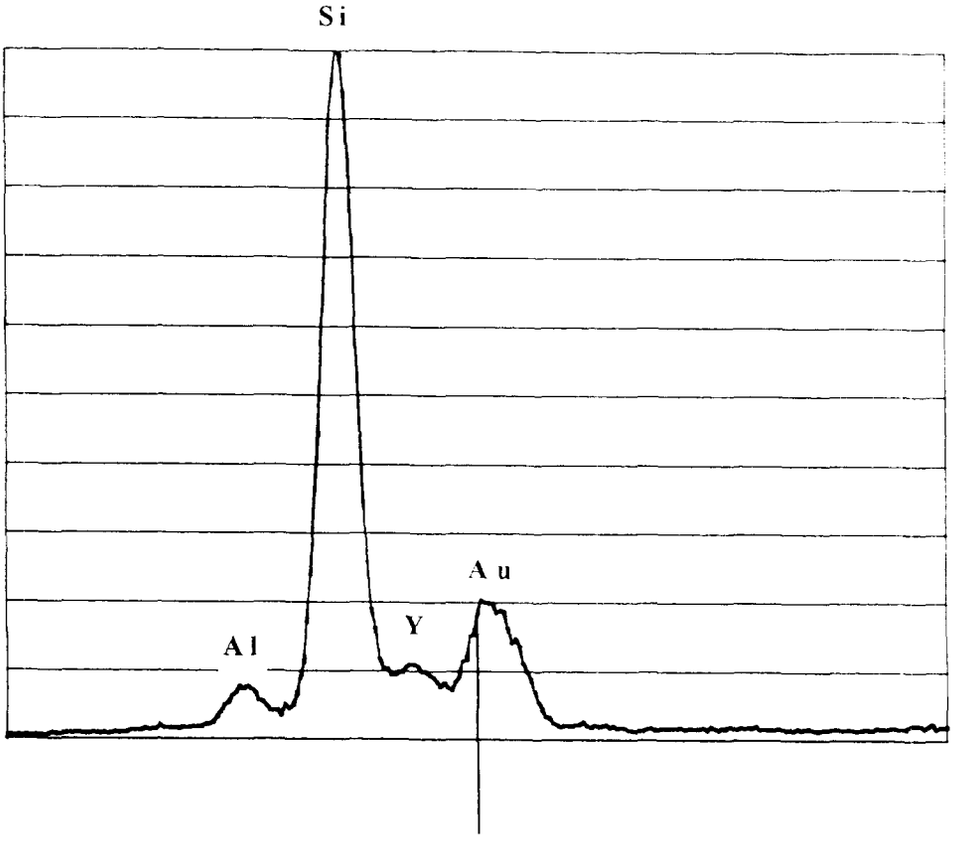

Fig. 14. EDAX analysis revealing that the regions between the crystals mostly contain Si with only trace contents of Y and Al.

approximately 50–100 μm in length and ~5 μm in diameter. The appearance of the yttrium silicate on the surface and the higher yttrium concentration in the crystals (comparison of Figs 13 and 14) indicates the outward diffusion of the yttrium element (or yttrium oxide), which preferentially reacts with the SiO_2 to form the needle-like crystalline silicate and continues to grow at the expense of the surrounding yttrium. Minor amounts of yttrium aluminate garnet (YAG) were observed only in the specimen with 20% additives oxidized at 1350 °C for longer than 30 h.

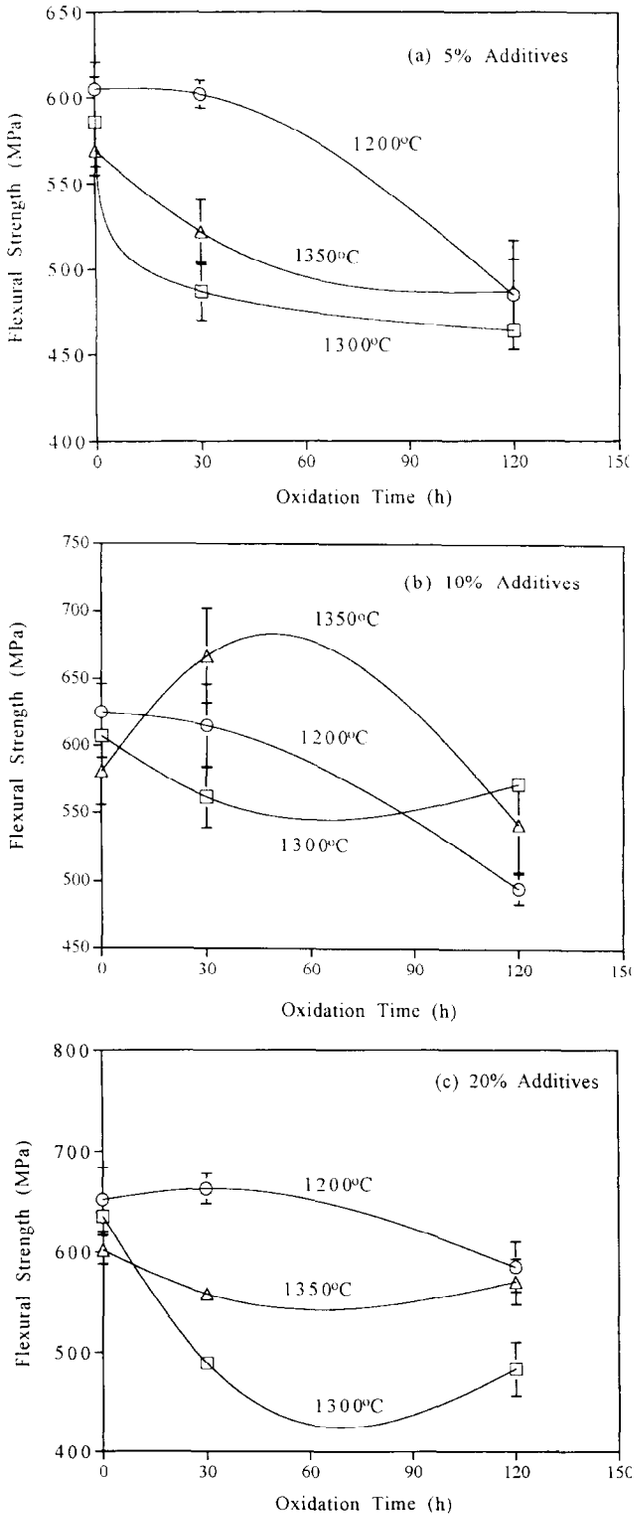

Fig. 15. Room-temperature flexural strength of the SiC ceramic containing (a) 5 wt%, (b) 10 wt% and (c) 20 wt% additives vs the oxidation soaking period at varying temperatures.

In many investigations, the activation energy for SiC oxidation will increase considerably at higher temperatures due to the crystallization of the amorphous SiO_2 scale. However, in the present study, no cristobalite crystalline phase was formed; instead, the yttrium silicate (and trace content of YAG) was formed which did not cause any considerable increase in activation energy (Fig. 5), suggesting that the in-diffusion rate of oxygen remained similar regardless of the formation of the crystalline phases. The actual reason for the localized crystallization and corresponding activation energy of oxidation is not clear. One possible explanation is the formation of the porous network in the oxide scale which facilitates the oxidant diffusion rate. This effect may thus compensate to some extent the decreased in-diffusion rate of oxygen due to the partially crystallized oxide scale to form needle-shaped $Y_2Si_2O_7$ and YAG phases.

3.4 Flexural strength

The influence of oxidation on the average flexural strength of the SiC–Al_2O_3–Y_2O_3 ceramics containing

Fig. 16. Large voids formation (see arrows) on the SiC substrate directly underneath the oxide scale.

various amounts of sintering additives is shown in Fig. 15. The bars indicate the standard deviation for the measured strength. Initially, at a soaking time of zero, the strength is relatively similar for each group of additive fraction irrespective of the oxidation temperature. The average flexural strength of the SiC ceramics increased with increasing additive content from ~580 MPa for 5 wt% to 606 MPa for 10 wt%, and increased further to 670 MPa for 20 wt%. With an increase in soaking time, the flexural strength degraded somewhat with oxidation at all temperatures, except an incidentally increased strength for 10 wt% additive oxidation at 1350°C for 30 h (Fig. 15(b)). This decrease in strength on oxidation is believed to be due to the pit formation on the surface which may act as strength-limiting flaws, particularly when the pits are large.

After oxidizing for as long as 120 h, a further strength degradation is less pronounced in comparison with the strength after 30-h oxidation. A slight increase in strength was occasionally seen for additive fractions greater than 10 wt% at temperatures ≥1300°C. The reason for these findings on strength behaviour is not known. It might be considered as the contribution of the formation of the needle-shaped crystals on the surface which could somehow act as a reinforcing phase.

Figure 16 shows a fractured surface examination for the specimen with 5 wt% additives at 1350°C for 30 h. The large voids (arrows) appeared to be present 10 μm underneath the oxide scale, having a dimension of 20–30 μm in diameter. These voids can act as fracture origins. These subsurface voids were most likely formed due to initial specimen preparation as previously reported[20] and were believed to be effective in the deterioration of the strength. If this argument is true, the morphology of the initially-prepared specimen surface could be responsible to a certain extent for the strength behaviour, particularly when the surface pits due to oxidation are below some critical size. Additionally, the presence of interconnected pores at the SiC/oxide interface (Fig. 10) may play an important role in transferring load. In this case, the oxide scale may only be a poor medium for bearing load (due primarily to decreased load-bearing area) and the strength behaviour may therefore be simply regarded as a microstructure dependence of the SiC itself.

4 SUMMARY AND CONCLUSIONS

Oxidation kinetics associated with the microstructural evolution of the oxide scale in the system SiC–Al_2O_3–Y_2O_3 ceramics were investigated. The oxidation of the SiC ceramics can be described using the classical parabolic rate model. The rate-limiting step for the oxidation of the SiC–Al_2O_3–Y_2O_3 ceramics is the in-diffusion of oxygen molecules through the oxide film as supported by a similar activation energy value as observed in the oxidation of silica. The apparent activation energy of oxidation decreases with an increasing content of sintering additives; 128 kJ/mol, 114 kJ/mol and 91 kJ/mol for 5 wt%, 10 wt% and 20 wt% additive fractions, respectively. This decrease in activation energy is probably due to the lowering of the devitrification temperature by reducing the oxide viscosity, which further facilitates the oxidant in-diffusion rate. The formation of crystalline phases, i.e. $Y_2Si_2O_7$ and YAG, does not cause an increase in activation energy due to limited diffusion rates and this may be compensated by the formation of a porous structure within the oxide scale. The oxide scale is essentially a porous composite structure rather than a dense structure and would be expected to be a poor protective layer for high-temperature oxidation-resistant applications. The flexural strength of the SiC ceramics decreases somehow with oxidation and the strength behaviour is a complex function of oxidized surface morphology, as well as the microstructure of the SiC itself underneath the scale.

ACKNOWLEDGEMENTS

The author gratefully acknowledges the support of the Ministry of Economic Affairs, ROC, by funding this research under contract No. 843KG2230. The X-ray difraction analysis by Dr I. J. Lin is also acknowledged.

REFERENCES

1. OMORI, M. & TAKEI, H., Preparation of pressureless-sintered SiC–Al_2O_3–Y_2O_3. *J. Mater. Sci.*, **23** (1988) 3744–3749.
2. LEE, S. K., KIM, Y. C. & KIM, C. H., Microstructural development and mechanical properties of pressureless-sintered SiC with plate-like grains using Al_2O_3–Y_2O_3 additives. *J. Mater. Sci.*, **29** (1994) 5321–5326.
3. LIU, D. M., FU, C. T. & JOU, Z. C., Microstrcture and high temperature flexural strength of SiC–Al_2O_3–Y_2O_3 ceramics. *J. Mater. Sci. Lett.*, **14** (1995) 1327–1328.
4. SINGHAL, S. C., Oxidation kinetics of hot-pressed silicon carbide. *J. Mater. Sci.*, **11** (1976) 1246–1253.
5. HINZE, J. W., TRIPP, W. C. & GRAHAM, H. C., The high-temperature oxidation of hot-pressed silicon carbide. In *Mass Transport Phenomenon in Ceramics*, ed. A. R. Cooper & A. H. Heuer. Plenum Publishing Co., New York, 1975, pp. 409–428.
6. ADAMSKY, R. F., Oxidation of silicon carbide in the temperature range 1200–1500°C. *J. Phys. Chem.*, **63** (1959) 305–307.

7. MIESKOWSKI, D. M., MITCHELL, T. E. & HEUER, A. H., Bubble formation in oxide scale. *J. Am. Ceram. Soc.*, **67**(1) (1984) c17–c18.
8. COSTELLO, J. A. & TRESSLER, R. E., Oxidation kinetics of hot-pressed and sintered α-SiC. *J. Am. Ceram. Soc.*, **64**(5/6) (1981) 327–331.
9. PULTZ, W. W., Temperature and oxygen pressure dependence of silicon carbide oxidation. *J. Phys. Chem.*, **71**(13) (1967) 4556–4558.
10. NARUSHIMA, T., GOTO, T. & HIRAI, T., High-temperature passive oxidation of chemically vapour deposited silicon carbide. *J. Am. Ceram. Soc.*, **72**(8) (1989) 1386–1390.
11. LEVIN, E. M. ROBBINS, C. R. & McMURDIE, H. F., Figure 2344 in *Phase Diagrams for Ceramists*, ed. M. K. Reser. Columbus, OH, 1969.
12. LIU, D. M., Crack propagation and interfacial property in SiC– Al_2O_3–Y_2O_3 ceramics. *J. Mater. Sci. Lett.*, **15** (1996) 1077–1078.
13. NORTON, F. J., Permeation of gaseous oxygen through vitreous silica. *Nature*, **191** (1961) 4789.
14. COSTELLO, J. A. & TRESSLER, R. E., Oxidation kinetics of silicon carbide crystals and ceramics — I. In dry oxygen. *J. Am. Ceram. Soc.*, **69**(9) (1986) 674–681.
15. SINGHAL, S. C. & LANGE, F. F., Effect of alumina content in the oxidation of hot-pressed SiC. *J. Am. Ceram. Soc.*, **58**(9-10) (1975) 433–435.
16. GROVE, A. S., LEISTRIKO, O., Jr & SAH, C. T., Redistribution of acceptor and donor impurities during thermal oxidation of silicon. *J. Appl. Phys.*, **35**(9) (1964) 2695–2704.
17. ZHANG, S. L. & D'HEURLE, F. M., Note on the linear–parabolic law of phase formation. *Phil. Mag. A.*, **64**(3) (1991) 619–627.
18. SCHIROKY, G. H., Oxidation behaviour of chemically vapour deposited silicon carbide. *Adv. Ceram. Mater.*, **2**(2) (1987) 137–141.
19. SINGHAL, S. C., Thermodynamics and kinetics of oxidation hot-pressed silicon carbide. *J. Mater. Sci.*, **11** (1976) 500–509.
20. LIU, D. M., FU, C. T. & LIN, L. J., Influence of machining on the strength of SiC–Al_2O_3–Y_2O_3 ceramic. *Ceram. Int.*, **22**(3) (1996) 267–270.